Supporting Information

Solar-irradiated carbon dots as high-density hot spots in sponge for high-efficient cleanup of viscous crude-oil spill

Yucheng Su,[a] Qing Chang,[a] Chaorui Xue,[a] Jinlong Yang,[a,b] and Shengliang Hu[a]*

[a] Research Group of New Energy Materials and Devices, North University of China, Taiyuan 030051, P. R. China.

[b] State Key Laboratory of New Ceramics and Fine Processing, Tsinghua University, Beijing 100084, P. R. China.

*Corresponding Author, E-mail: hsliang@yeah.net

1. Experimental details

1.1 Materials and Chemicals

Commercial porous melamine sponge were purchased from Ledian furniture company of China without further treatment. PDMS [$(C_2H_6OSi)_n$], formic acid (88v/v%) and hydrogen peroxide (30v/v%) was purchase form Aladdin reagent. Absolute ethyl alcohol (AEA) and ethyl acetate (EA) was purchased from Damao chemical reagent factory of China. All chemical reagents were dierectly used with no further purification.

1.2 Methods

CDs were obtained by selective oxidation etching method using coal tar pitch as precursors and the mixture of hydrogen peroxide and formic acid as the oxidizing agent with a final optimization reported in the literature[1]. As-prepared 50 mg of CDs' powder was further dispersed in 10 mL of absolute ethyl alcohol by ultrasonic agitation for 10 min in room temperature to obtain CDs suspension. Subesequently, 50 mg of PDMS was added into 50 mL of the EA by stiring for 10 min to achieve the mixed solution of PDMS-EA solution. The resultant CDs suspension and PDMS-EA solution were evenly mixed to achieve PDMS-CDs-EA solution. The fabrication processes of DC-S and CR-S were illustrated in Figure 1a. For DC-S, CPS was firstly soaked in the PDMS-CDs-EA solution for 2 hours, then put into a drying oven and heated at 60 ℃ for 4 hours to obtain DC-S. For CR-S, CPS was firstly soaked in 30 mL of the PDMS-CDs-EA solution prepared above, afterwards all of them was transferred into a 50 mL of poly (tetrafluoroethylene) Teflon-lined autoclave and

heated in an oven at 150 °C for 2 hours. After cooling to room temperature, CPS was taken out and subsequently put into the drying oven and heated at 60 °C for 4 hours to obtain CR-S.

1.3 Sample characterization

Absorption spectra were collected on a UV-Vis-NIR spectrophotometer (Shimadzu UV3600) with an integrated sphere in the range of 250–2,500 nm wavelengths. Scanning electron microscope (SEM) observations were performed in a Hitachi S-4800 microscope. The contact angle tests of samples were measured by a contact angle system (Dataphysics, OCA20, Germany). The X-ray photoelectron spectroscopy (XPS, PHI 5000 Versaprobe-II Focus) was used to confirm the chemical modifications of samples.

1.4 Photothermal test and curde oil adsorption

Artificial seawater (3.5 wt% NaCl solution) and crude oil were put into a beaker to obtain a mixture for an accidental crude oil spill simulation. A solar simulator (CEL-HXUV300, CEAULIGHT, China) with an intensity of 100 mW m^{-2} (one Sun) was employed in the experiment. An infrared (IR) camera were employed to record the top surface temperature. The temperatures at the top surface and bottom surface of the sample were measured using a dual-channel thermometer (Xinster HT-9815) with thermocouple wire in direct contact with the top surface and bottom surface. The DC-S or CR-S sponge with a shape of 2 cm (length) × 2 cm (width) × 0.5 cm (thickness) was placed on a home-made thermally insulating expanded polystyrene (EPS) foam plate for characterizing photothermal performance, and on the surface of the prepared

mixture of crude oil and seawater for characterizing adsorption performance. All of experiments were conducted at room temperature. To quantitatively estimate adsorption capability of oil, the sample sponge was hung on a holder that was linked to an electrical balance[2]. The weight change of the sample sponge was real time monitored and recorded. The adsorption capacity *(Q)* of curde oil was determined by equation (S1) and the corresponding adsorption rate *(V)* was calculated by equation (S2)

$$Q = \frac{\dot{m} - m}{m}$$

(S1)

$$V = \frac{Q}{t}$$

(S2)

where Q is the adsorption capacity of sample sponge (g•g^{-1}); $\dot{m}$ is the mass of sample sponge after adsorbing curde oil (g); m is the initial mass of sample sponge (g); V is the adsorption rate of sample sponge; t is the adsorption time of sample sponge (min).

For cycle performance measurement, as-prepared sample sponge was first oil-saturated by above 15 min one-sun irradiation and subsequently manual squeezing was applied to force out the crude oil from the oil-saturated sponge. The same sample sponge was repeatedly used for the crude oil adsorption and released again for multiple times. It should be mentioned that the oil-saturated sponge requires to be qucikly squeezed to release all of absorbed oils as adsorption completed under solar irradiation. In the meantime, the crude oils adsorbed in sponge still kept high temperature and low viscosity.

1.5 Heat transfer simulation in microchannel

The heat transfer modes of microchannels involved in heat conduction (q_{hm}) and thermal radiation (q_{rm}) of photothermal materials as well as heat conduction (q_{hg}), thermal convection (q_{tg}) and thermal radiation (q_{rg}) of gas in the channel. Thus, the heat energy (E_m) transferring to the bottom surface can be described as.

$$E_m = q_{hm} + q_{rm} + q_{hg} + q_{tg} + q_{rg} \tag{S3}$$

Assuming that heat conduction in microchannels was two-dimensional steady-state heat conduction and no inner heat source, heat conduction was determined by equation (S4).

$$q_{hm} + q_{hg} = \rho_m c_{pm} \frac{\partial T(x,y)}{\partial t} + \rho_g c_{pg} \frac{\partial T(x,y)}{\partial t} \tag{S4}$$

Considering that thermal convection of gas in microchannels was also two-dimensional steady-state, thermal convection was determined by equation (S5).

$$q_{tg} = \rho_g c_{pg} \left(\frac{\partial T}{\partial t} + u \frac{\partial T}{\partial x} + v \frac{\partial T}{\partial y} \right) \tag{S5}$$

Radiative heat transfer only considers the heat transfer between photothermal materials and crude oil and the heat transfer between gas and crude oil. Therefore, thermal radiation of photothermal materials and thermal radiation of gas in the microchannels was determined by equation (S6).

$$q_{rm} + q_{rg} = \frac{\left(\frac{T_t}{100}\right)^4 - \left(\frac{T_b}{100}\right)^4}{\frac{1}{\varepsilon_t} + \frac{1}{\varepsilon_b} - 1} + \frac{\left(\frac{T_g}{100}\right)^4 - \left(\frac{T_b}{100}\right)^4}{\frac{1}{\varepsilon_g} + \frac{1}{\varepsilon_b} - 1} \tag{S6}$$

In microchannels, the flow of gas was ignored. In the meantime, given to the minor amount of gas in microchannel, the temperature of the gas can be set to the same as the initial temperature of the bottom surface. Hence, thermal convection (q_{tg}) and thermal radiation (q_{rg}) of gas in the channel were ignored. As a result, heat

energy (E_M) transferring to the bottom surface can be simplified as:

$$E_M = \rho_m c_{pm}\frac{\partial T(x,y)}{\partial t} + \rho_g c_{pg}\frac{\partial T(x,y)}{\partial t} + \frac{\left(\dfrac{T_t}{100}\right)^4 - \left(\dfrac{T_b}{100}\right)^4}{\dfrac{1}{\varepsilon_t} + \dfrac{1}{\varepsilon_b} - 1} \qquad (S7)$$

where ρ_m, ρ_g are mass density of photothermal materials and air, respectively; c_{pm}, c_{pg} are specific heat of photothermal materials and air, respectively; T_t, T_b are the balance temperature of the top surface (65 ℃) and the initial temperature of the bottom surface (25 ℃), respectively; $\varepsilon_b, \varepsilon_t$ are emissivity of CPS and photothermal materials, respectively. For the model using heat conduction as the main heat transfer mode, reduced graphene oxide (rGO) with high thermal conductivity was considered as photothermal materials upon CPS for comparison. The simulated results were showed in Figure S11.

2. Supporting results
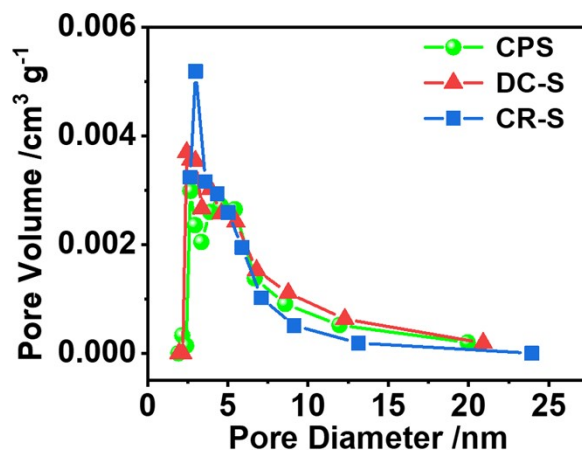
Figure S1. Pore size distributions of CPS, DC-S and CR-S
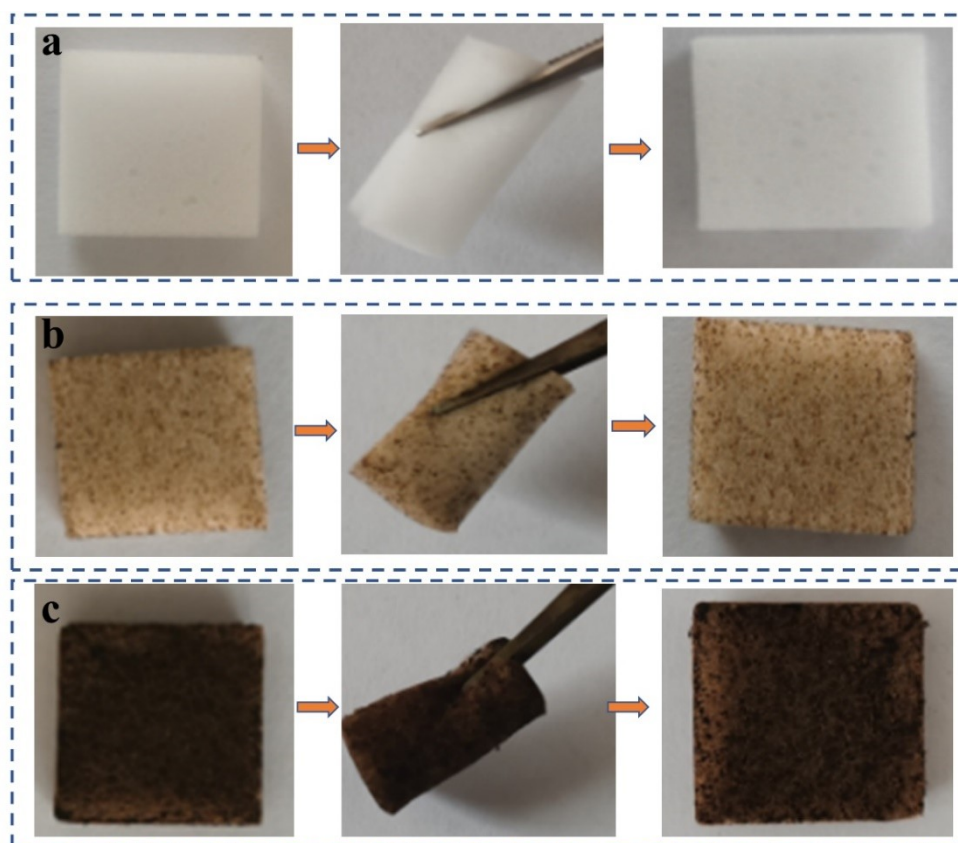
Figure S2. Photographs of the mechanical strength and bend toughness of CPS (a), DC-S (b) and CR-S (c)
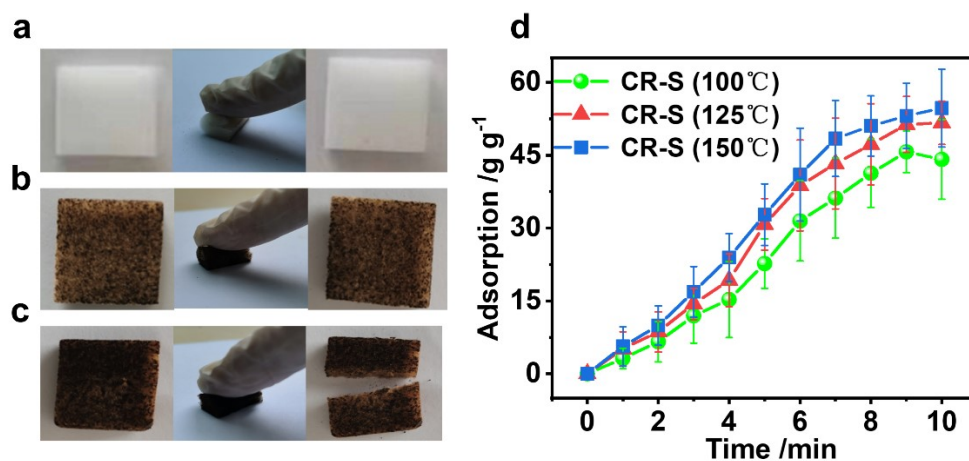
Figure S3. (a-c) The photographs of the mechanical properties of CPS from 150 ℃ (a), CR-S from 150 ℃ (b) and CR-S from 180 ℃ (c); (d) Adsorption performances of CR-S prepared at 100, 125 and 150 ℃ under 1 sun irradiation.
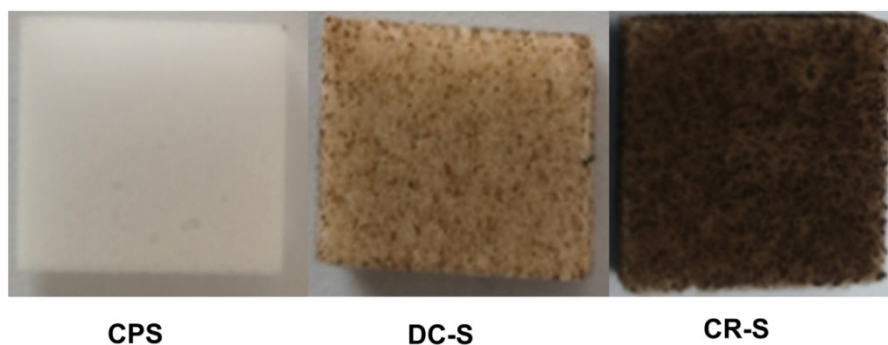

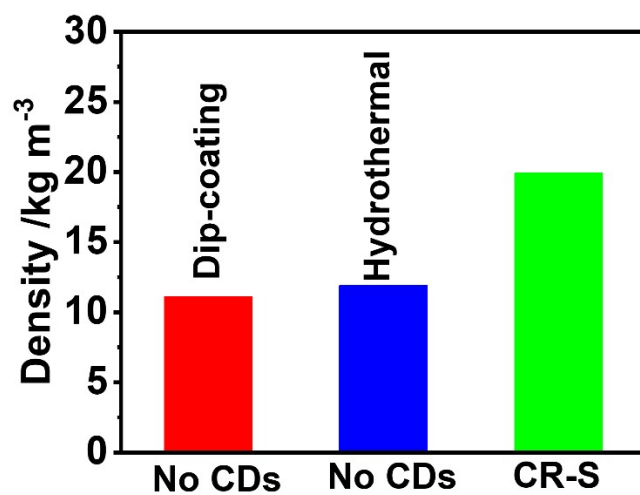
Figure S4. The photographs of CPS, DC-S and CR-S

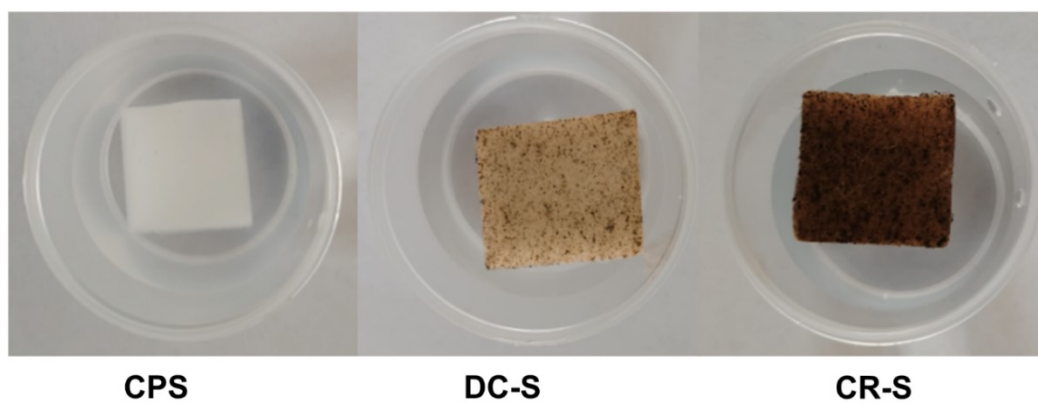**Figure S5.** The effect of PDMS on the density of sample sponges treated by dipping and hydrothermal method, respectively

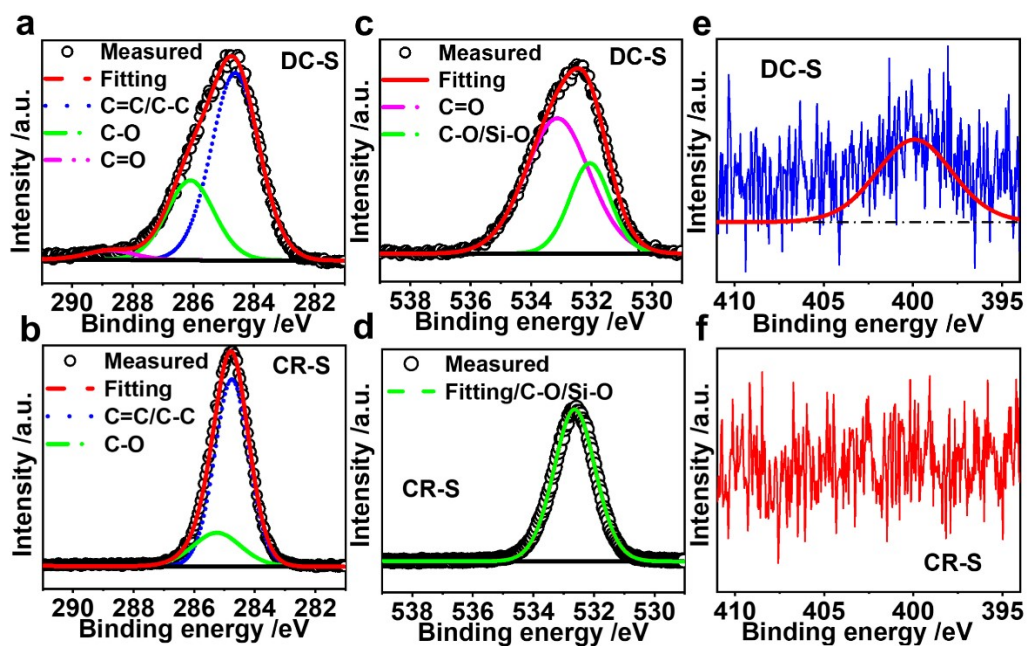**Figure S6.** The photographs of CPS, DC-S and CR-S floated on seawater for above 24 hours.

Figure S7. (a-b) XPS C1s spectra of DC-S and CR-S; (c-d) XPS O1s spectra of DC-S and CR-S; (e-f) XPS N1s spectra of DC-S and CR-S
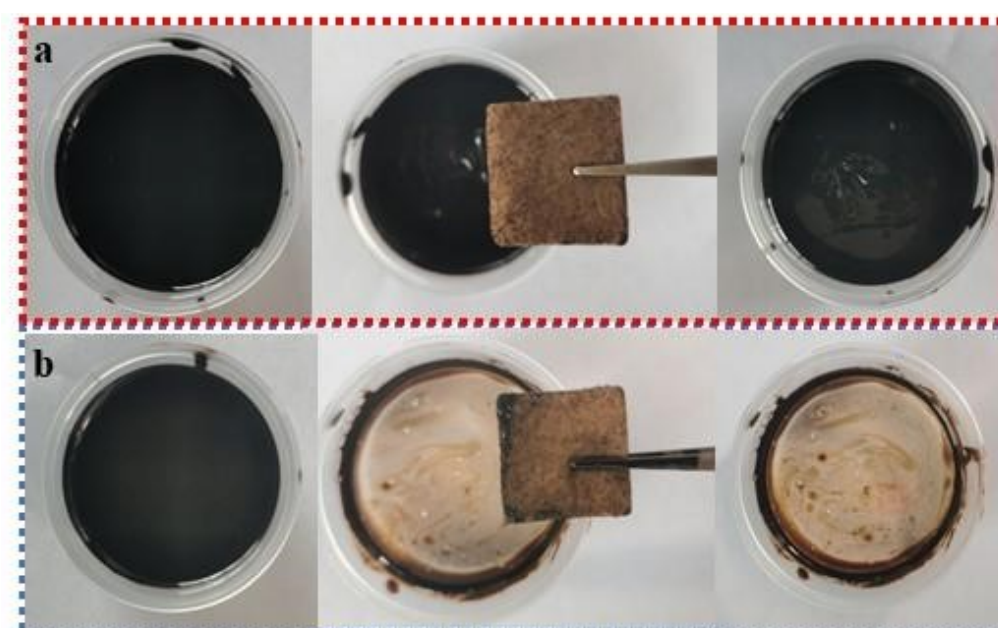

Figure S8. (a) Adsorption photographs of CR-S at room temperature without light irradiation; (b) Adsorption photographs of CR-S with 1 sun irradiation
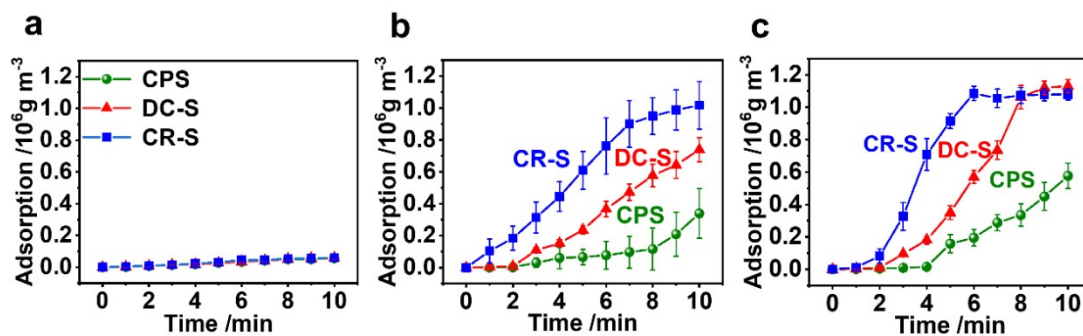
Figure S9. The volumetric capacity of CPS, DC-S and CR-S for crude oil under dark condition (a), one sun irradiation (b) and two sun irradiation (c).
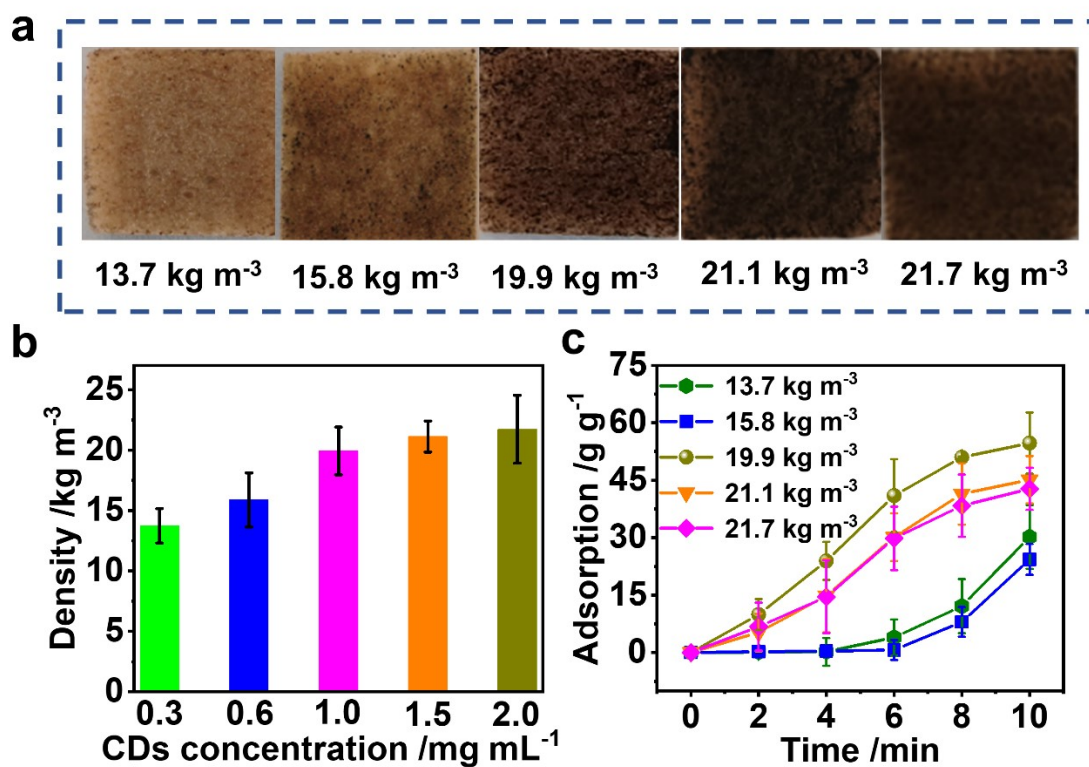

Figure S10. Photographs of sample sponges prepared in different concentrations of CDs (a) and the corresponding densities (b); (c) Adsorption capacities of sample sponges for crude oil under one irradiation
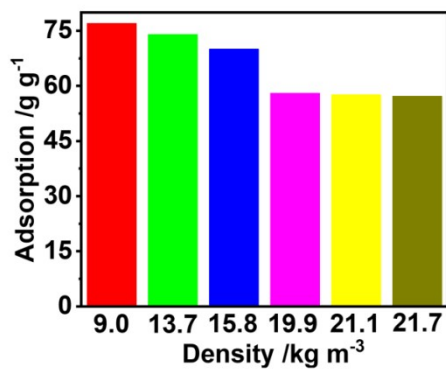
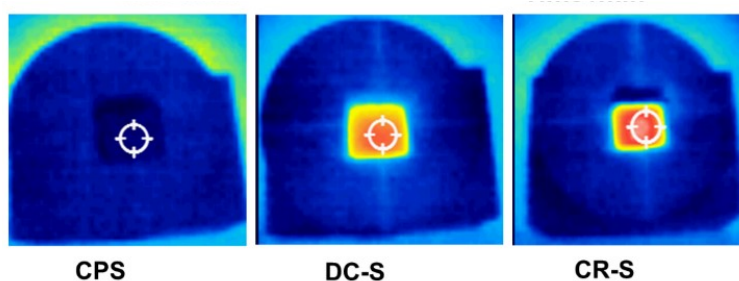**Figure S11.** The dependence of oil-saturated capacity with sample sponge density

Figure S12. The infrared images of surface temperature distribution of DC-S and CR-S under I sun irradiation
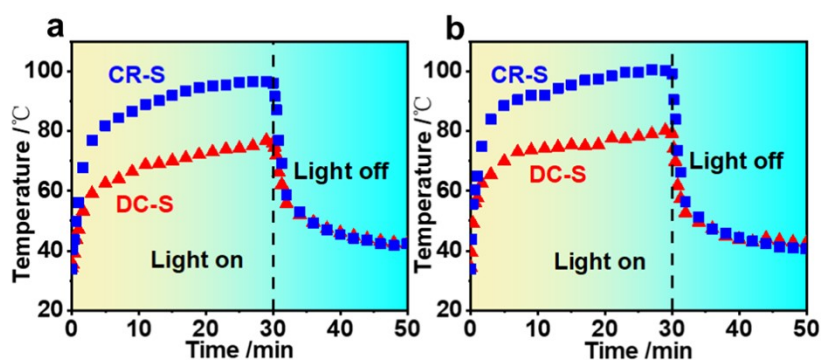

Figure S13. (a) Time-dependent temperature changes of the upper surface of DC-S and CR-S under 2 sun irradiation; (b) Time-dependent temperature changes of the bottom surface of DC-S and CR-S under 2 sun irradiation.
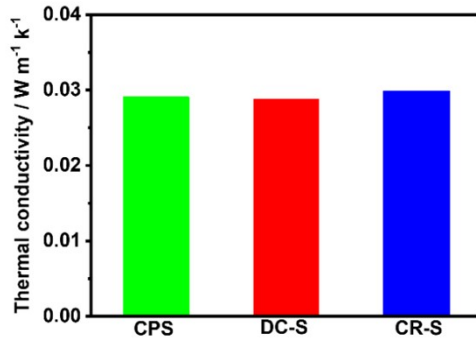
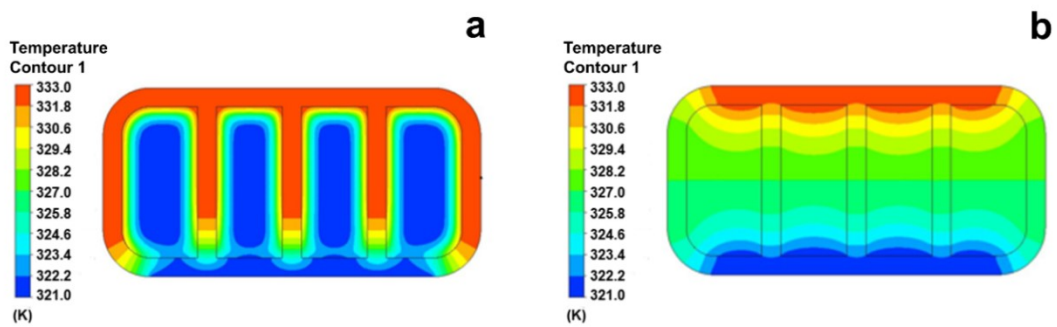**Figure S14.** Thermal conductivity of CPS, DC-S and CR-S.

Figure S15. (a) Temperature profile of photothermal materials using heat conduction as main heat transfer mode; (b) Temperature profile of photothermal materials using thermal radiation as main heat transfer mode
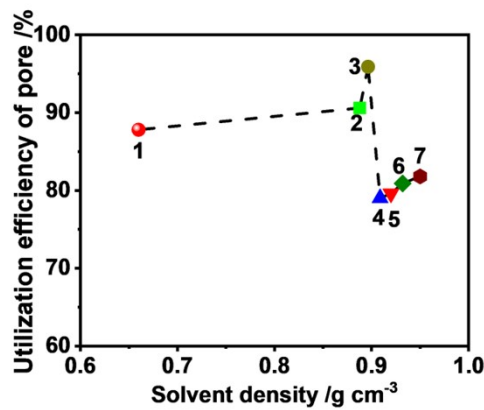

Figure S16. The utilization efficiency of pore space of sample sponge for adsorbing different oils and organic solvents

Table S1. Comparisons of adsorption performance of CR-S with reported absorbents

Work	Photothermal materials	Adsorption carrier	Adsorption mass (g.g^{-1})	Reference
R1	rGO	sponge	**20.85**	3
R2	rGO	/	**38**	4
R3	GA-GuFeSe$_2$	/	**18.63**	5
R4	PPy	sponge	**29.2**	6
R5	PDA	sponge	**20**	7
R6	PPy-PDA-Bn	sponge	**45**	8
R7	PDA	sponge	**11.2**	9
R8	Ti$_3$C$_2$T$_X$ MXene	sponge	**40**	10
R9	Fe$_3$O$_4$	sawdust	**7.83**	11
R10	MoS$_2$	sponge	**22**	12
R11	Ti$_3$C$_2$Tx	wood	**24.5**	13
This work	CDs	sponge	**58.8**	/

References

1. X. Meng, Q. Chang, C. Xue, J. Yang and S. Hu, *Chem. Commun.*, 2017, **53**, 3074-3077.

2. J. Chang, Y. Shi, M. Wu, R. Li, L. Shi, Y. Jin, W. Qing, C. Tang and P. Wang, *J. Mater. Chem. A*, 2018, **6**, 9192-9199.

3. Z. Zhang, H. Liu and W. Qiao, *Colloid Surface A*, 2020, **589**, 124433-124444.

4. O. Bagoole, M. M. Rahman, S. Shah, H. Hong, H. Chen, A. Al Ghaferi and H. Younes, *Environ. Sci. Pollut. Res. Int.*, 2018, **25**, 23091-23105.

5. A. Sun, X. Hou and X. Hu, *Nano Energy*, 2020, **70**, 104511-104518.

6. C. Yang, B. Bai, Y. He, N. Hu, H. Wang and Y. Suo, *Ind. Eng. Chem. Res.*,

2018, **57**, 4955-4966.

7.	C. Zhang, M.-B. Wu, B.-H. Wu, J. Yang and Z.-K. Xu, *J. Mater. Chem. A*, 2018, **6**, 8880-8885.

8.	X. Wu, S. Li, J. Huang, Z. Chen, W. Cai and Y. Lai, *iScience*, 2021, **24**, 102665-102680.

9.	J. Yang, P. Xu, Y. Yao, Y. Li, B. Shi, X. Jia and H. Song, *Mater. Des.*, 2020, **195**, 108979-108988.

10.	C. Gong, J. Lao, B. Wang, X. Li, G. Li, J. Gao, Y. Wan, X. Sun, R. Guo and J. Luo, *J. Mater. Chem. A*, 2020, **8**, 20162-20167.

11.	Z. Yin, Y. Li, T. Song, M. Bao, Y. Li, J. Lu and Y. Li, *J. Cleaner Prod.*, 2020, **253**, 120058-120070.

12.	M. Yu, P. Xu, J. Yang, L. Ji and C. Li, *Adv. Mater. Interfaces*, 2020, **7**, 1901671-1901680.

13.	C. Cai, Z. Wei, Y. Huang and Y. Fu, *Chem. Eng. J.*, 2021, **421**, 127772-127784.